Magnetic properties of hexagonal Laves-phase $Zr(Cr_{1-x}Fe_x)_2$ compounds

2001 J. Phys.: Condens. Matter 13 8415

(http://iopscience.iop.org/0953-8984/13/36/314)

INSTITUTE OF PHYSICS PUBLISHING JOURNAL OF PHYSICS: CONDENSED MATTER

J. Phys.: Condens. Matter **13** (2001) 8415–8434 PII: S0953-8984(01)24696-7

Magnetic properties of hexagonal Laves-phase $Zr(Cr_{1-x}Fe_x)_2$ compounds

J A H Coaquira and H R Rechenberg[1]

Instituto de Física, Universidade de São Paulo, C.P. 66318, 05315-970 São Paulo, Brazil

Received 10 May 2001
Published 23 August 2001
Online at stacks.iop.org/JPhysCM/13/8415

Abstract

$Zr(Cr_{1-x}Fe_x)_2$ samples with the C14 structure were prepared in an arc furnace for $x = 0.2-0.85$. Magnetization, ac susceptibility and Mössbauer spectra were measured in the 4.2–300 K temperature interval. Saturation magnetic moments were obtained from magnetization data and iron moments were obtained from Mössbauer spectra; the Cr moment was found to be negligible. A new environment-dependent model for the formation of Fe moments was proposed. Arrott plots showed that long-range magnetic order only occurs for $x > 0.7$. Spin glass properties were studied in detail for $x \leqslant 0.7$. Samples with $x = 0.8-0.85$ were ferromagnetic with a re entrant spin glass transition. A magnetic-phase diagram was drawn for this system.

1. Introduction

Transition metals and their alloys have been at the forefront of basic and applied research since the earliest days of modern magnetism. In addition to simple alloys obtained by mixing two or more such metals, an alternative framework for investigating 3d-electron magnetism is provided by intermetallic compounds formed with other kinds of elements. Among these, the Laves-phase compounds AB_2, with B a transition metal, have been most extensively investigated in the last decades. Leaving aside those compounds in which A is a magnetic rare earth ion, there remain a large number of systems with A as an element of the IIIB to VB groups, such that only 3d-element atoms are potentially magnetic. It has been found that, while AFe_2 compounds are generally ferromagnetic, all ACo_2 and ANi_2 compounds are Pauli paramagnets [1–4]. Since the B sites in the AB_2 lattice can usually accommodate a random mixture of two different transition-metal atoms, the question that naturally arises is how magnetism sets in upon gradual substitution of Co or Ni by Fe or other elements, or conversely, how it is destroyed when Fe in AFe_2 is diluted with other transition elements or with Al or Si. These problems have been investigated in great detail [3, 4]. It has been found, for example, that the critical concentration x_c for the onset of long-range ferromagnetic order

[1] To whom correspondence should be addressed.

0953-8984/01/368415+20$30.00

was 0.1 for $Y(Co_{1-x}Fe_x)_2$, and 0.5 for $Zr(Co_{1-x}Fe_x)_2$. This difference suggests that YCo_2 is a more strongly enhanced Pauli paramagnet than $ZrCo_2$, a result that was confirmed by electronic structure calculations [5]. On the other hand, it has been shown by Mössbauer and susceptibility measurements that, in the above-mentioned pseudobinary systems, localized moments start building up in a concentration range below x_c and freeze at low temperatures, exhibiting mictomagnetic behaviour [3, 6].

In contrast to the Co–Fe or Fe–Al-based Laves-phase alloys, little is known about the corresponding Cr–Fe system. $Y(Cr_{1-x}Fe_x)_2$ only exists in a limited concentration range, and for $Zr(Cr_{1-x}Fe_x)_2$ only fragmentary magnetic data have been reported [7−11]. One reason for this apparent lack of interest in the $Zr(Cr_{1-x}Fe_x)_2$ system might be the structural changes it undergoes upon varying the Fe concentration. While the end compounds $ZrCr_2$ and $ZrFe_2$ crystallize in the cubic $MgCu_2$-type (C15) structure, a broad intermediate range $x \approx 0.2$–0.85 exhibits the hexagonal $MgZn_2$-type (C14) structure [12]. A similar situation occurs for $Zr(Fe_{1-x}Al_x)_2$, and for this system both the saturation magnetization and the Curie temperature show a discontinuous drop at the C15–C14 boundary [4].

In spite of its structural peculiarities, an investigation of the magnetism of the $Zr(Cr_{1-x}Fe_x)_2$ system was thought to be worthwhile by analogy with the $Cr_{1-x}Fe_x$ binary alloys, whose magnetic phase diagram is far from trivial. For increasing Fe concentration, the latter evolve from an antiferromagnetic/SDW state ($0 \leqslant x < 0.16$) through a spin glass state ($0.16 < x < 0.19$) to eventually become ferromagnetic [13]. Thus, antiferromagnetic coupling is expected to also play a role for Cr–Fe solid solutions in other structures, arousing the possibility of frustration-related phenomena. A spin glass phase has indeed been found, in narrow concentration ranges, in the Cr–Fe-based amorphous alloys $(Cr_{1-x}Fe_x)_{80}B_{20}$ [14] and $(Cr_{1-x}Fe_x)_{75}P_{16}B_6Al_3$ [15]. The present work deals with the magnetic properties of $Zr(Cr_{1-x}Fe_x)_2$ alloys in the C14 phase. Samples with this structure have been prepared for x ranging from 0.2 to 0.85. As will be apparent, this concentration interval was sufficiently broad to contain the most interesting part of the magnetic phase diagram, leaving 'ordinary' ferromagnetism to the narrow C15 range terminating at $ZrFe_2$.

2. Experimental details

$Zr(Cr_{1-x}Fe_x)_2$ samples with $x = 0.2$ to 0.85 were prepared by arc melting high-purity elements (3N5 Zr, 3N8 Fe, 4N7 Cr) under argon atmosphere. The samples were re-melted several times to ensure homogeneity. No further heat treatment was carried out, since preliminary x-ray measurements showed the samples to be single-phase. Powder x-ray diffractograms were obtained using Cu Kα radiation, with 0.05° steps in the $20° < 2\theta < 90°$ range. Magnetization measurements were carried out with a Foner-type vibrating sample magnetometer in applied fields up to 9 T and at temperatures between 4.2 and 300 K. AC susceptibility was measured in the 1.5–200 K temperature range using either a Hartshorn bridge coupled to a lock-in amplifier or a Quantum Design SQUID susceptometer. Mössbauer spectra were measured in a variable-temperature helium cryostat using a ^{57}Co(Rh) source kept at room temperature.

3. Results and discussion

3.1. Structural characterization

The powder x-ray diffraction data were analysed with the Rietveld refinement method. Analysis showed that all $Zr(Cr_{1-x}Fe_x)_2$ samples for $0.2 \leqslant x \leqslant 0.85$ were single-phase with the $MgZn_2$-type structure (space group $P6_3/mmc$). Refinement was carried out assuming a

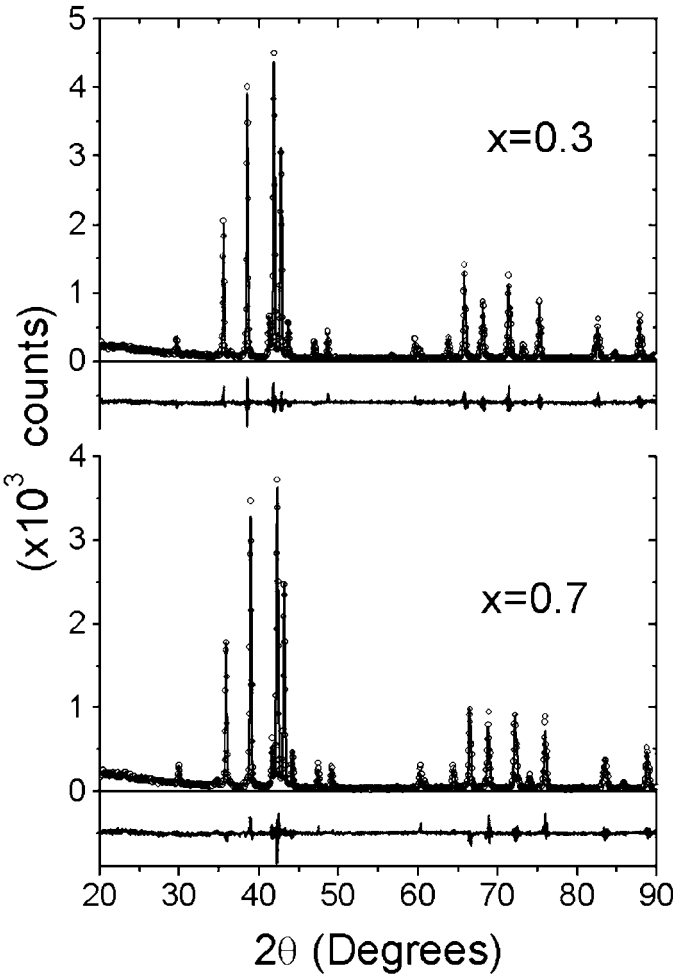

Figure 1. X-ray diffractograms of some C14-type $Zr(Cr_{1-x}Fe_x)_2$ samples (experimental points, Rietveld fits and difference curves are shown).

statistical distribution of Fe and Cr atoms on 2*a* and 6*h* sites, in accordance with neutron diffraction results [16]. A few additional weak reflections were assigned to α-Zr, amounting to less than 1% of the sample volume. Some x-ray diagrams are displayed in figure 1. Cell parameters decrease smoothly with increasing x, as shown in figure 2, and are in good agreement with published data [7, 8, 12, 16]. Further structural details have been reported elsewhere [17].

3.2. Magnetic and Mössbauer characterization at $T = 4.2$ K

Magnetization isotherms measured at 4.2 K are shown in figure 3. It is apparent that magnetic saturation is not reached up to 9 T applied field for any sample. A saturation magnetization value has been estimated by extrapolating the high-field part of the M versus H curves according to the expression [18]

$$M = M_S\left(1 - \frac{a}{H}\right) + \chi_0 H. \tag{1}$$

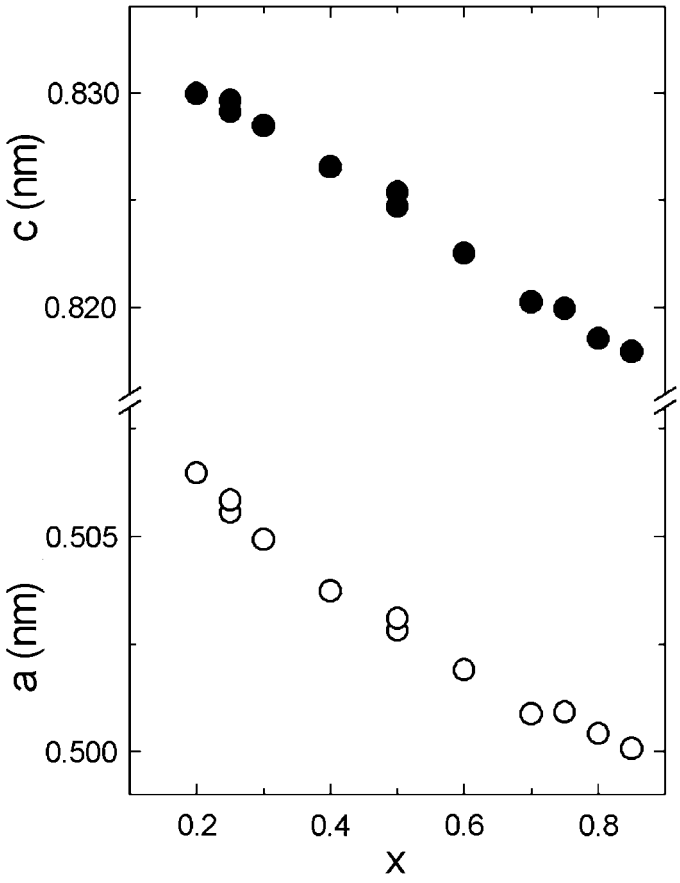

Figure 2. Measured lattice constants of C14-type $Zr(Cr_{1-x}Fe_x)_2$, $x = 0.2$ to 0.85.

The value $\chi_0 = 1.2 \times 10^{-5}$ emu g^{-1} Oe^{-1} was obtained by fitting the data for $x = 0.3$ and the same value was used for all samples. Resulting M_s data, expressed in Bohr magnetons/3d atom, are given in table 1.

Due to lack of saturation, it cannot be directly inferred from the magnetization data whether or not spontaneous magnetic ordering takes place in these alloys. However, the Arrott plots displayed in figure 4 clearly show that, for alloys with $x \geqslant 0.75$, the high-field part of the curves extrapolate to the positive vertical axis, indicating ferromagnetic order, whereas for $x \leqslant 0.7$ no spontaneous magnetization is present at 4.2 K.

Mössbauer spectra collected at $T = 4.2$ K are shown in figure 5. All samples with $x > 0.3$ exhibit magnetically split spectra with strongly overlapping lines. The occurrence of magnetic splitting $x \leqslant 0.7$ alloys indicates spin freezing, though without long-range magnetic order as shown by the magnetization data. Since the spectra are very nearly symmetrical, they could be fitted with a distribution of hyperfine fields without any quadrupole interaction. As was shown elsewhere [17], quadrupole interactions are too small (<0.3 mm s^1) to produce an appreciable effect in the presence of magnetic splitting. Isomer shift differences between the two unequivalent Fe sites 2*a* and 6*h*, on the other hand, are small and can only be resolved in

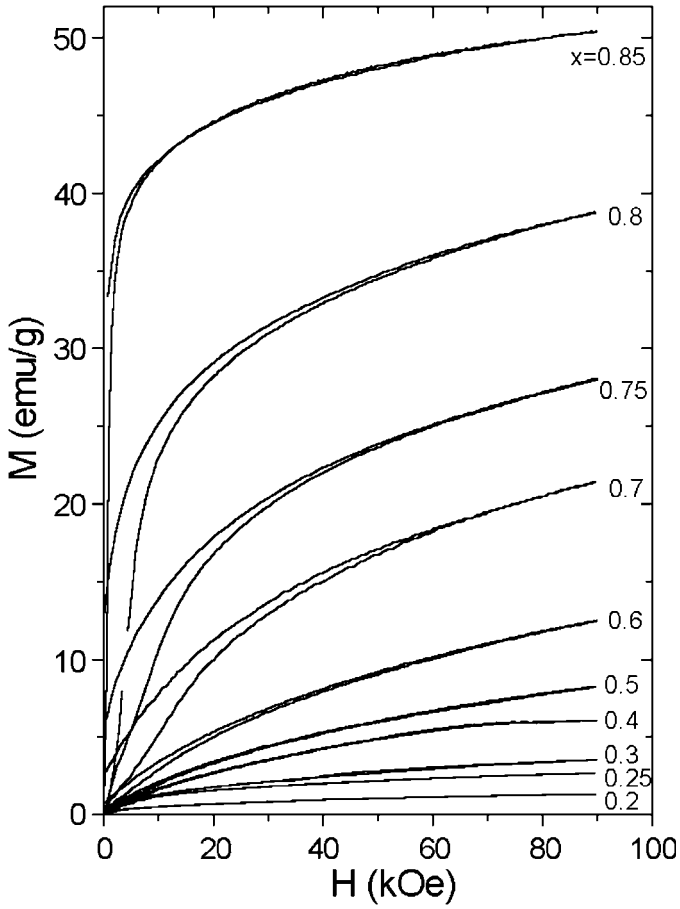

Figure 3. Magnetization curves of $Zr(Cr_{1-x}Fe_x)_2$ at $T = 4.2$ K.

Table 1. Concentration dependence of saturation moment μ_s, mean hyperfine field $\bar{B}_{hf}$, and Fe moment $\bar{\mu}_{Fe}$ calculated from $\bar{B}_{hf}$ using the conversion constant $A = 13.2$ T/μ_B Measuring temperature was $T = 4.2$ K.

x	0.3	0.4	0.5	0.6	0.7	0.75	0.8	0.85
μ_s (μ_B/3d atom)	0.05(2)	0.12(2)	0.17(1)	0.28(1)	0.47(2)	0.54(5)	0.75(5)	0.93(5)
$\bar{B}_{hf}$(T)	—	3.1(3)	5.1(3)	7.4(3)	9.7(3)	10.6(3)	11.9(3)	12.7(3)
$\bar{\mu}_{Fe}$ (μ_B/Fe atom)	—	0.23(2)	0.39(2)	0.56(2)	0.73(2)	0.80(2)	0.90(2)	0.96(2)

spectra without magnetic splitting. Similarly, the magnetically split spectra did not show any feature that could be assigned to differences between the 2*a* and 6*h* sites.

The average hyperfine fields $\bar{B}_{hf}$ calculated from the $P(B_{hf})$ distributions are given in table 1. The average Fe magnetic moment $\bar{\mu}_{Fe}$ can be estimated by assuming a proportionality law $B_{hf} = A\mu_{Fe}$ and taking $A = 13.2$ T/μ_B as determined from magnetization and hyperfine field data for ferromagnetic $ZrFe_2$ [7, 19]. The $\bar{\mu}_{Fe}$ values thus obtained are plotted in

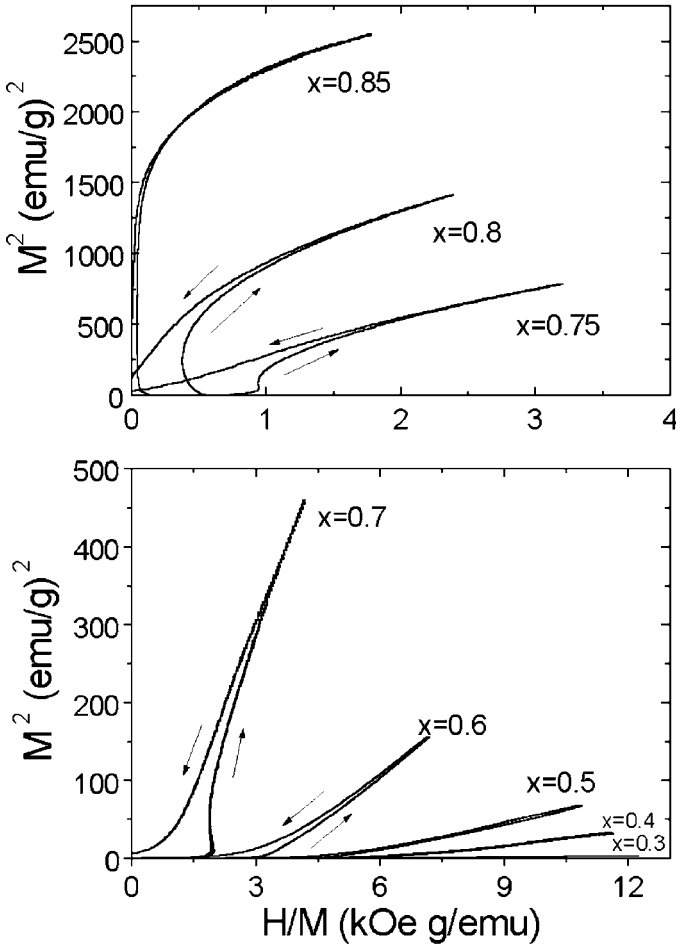

Figure 4. Arrott plots of $Zr(Cr_{1-x}Fe_x)_2$ at $T = 4.2$ K.

figure 6 along with the μ_s obtained from magnetization measurements. A striking feature of these results is the almost linear increase of $\bar{\mu}_{Fe}$ with Fe concentration up to $x = 0.8$, apparently extrapolating to zero at $x \approx 0.26$.

The gradual appearance of a magnetic moment with increasing concentration is usually associated with local environmental effects. The simplest, and often successful, phenomenological description of such effects is provided by the Jaccarino–Walker model, which postulates that an Fe (or Co) atom dissolved in a non magnetic matrix requires a minimum number of first neighbours of the same species to acquire its full moment, the moment being zero otherwise [20]. This model, however, is unable to account for the observed μ versus x behaviour in the present study. Instead, we shall make the following assumptions: an Fe atom will be magnetic if it has at least n_c Fe nearest neighbours, and its moment will be proportional to the excess number of Fe neighbours. We further assume an additional contribution of next-nearest Fe neighbours, proportional to their number. Thus, the moment of an Fe atom with n Fe first neighbours and m Fe second neighbors will be given by

$$\mu_{Fe}(n, m) = \mu_1(n - n_c) + \mu_2 m, \tag{2}$$

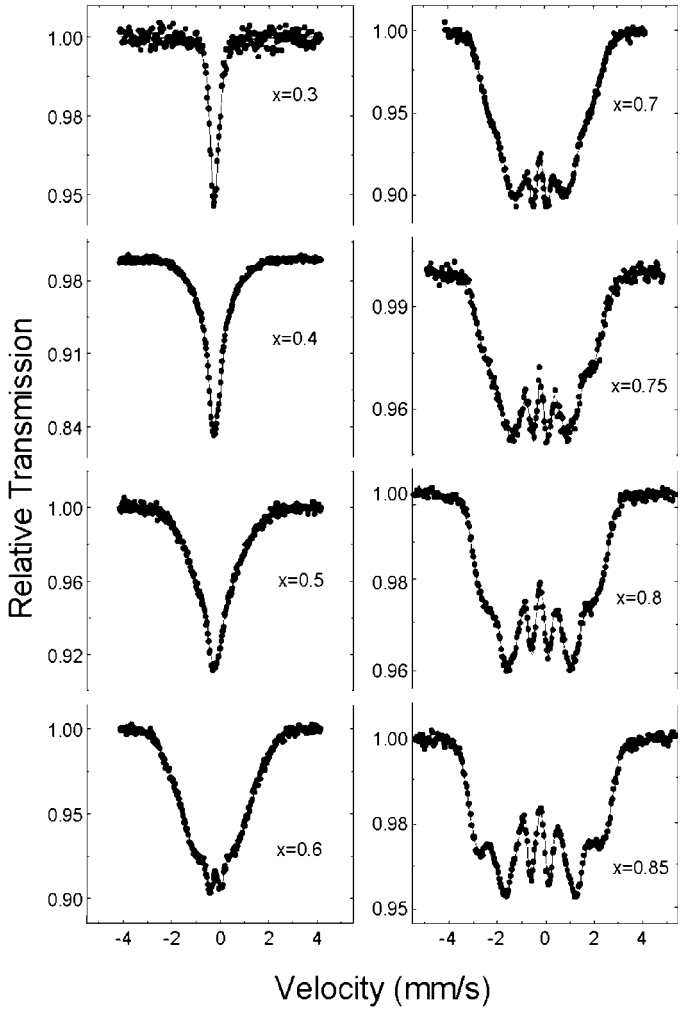

Figure 5. Mössbauer spectra of $Zr(Cr_{1-x}Fe_x)_2$ at $T = 4.2$ K (continuous lines are fits).

with the condition that the term proportional to μ_1 vanishes if $n < n_c$. In the C14 structure, $0 \leqslant n \leqslant 6$ and $0 \leqslant m \leqslant 12$ for both $2a$ and $6h$ sites, which will be considered equivalent for the present purpose. The average Fe moment is thus given by

$$\bar{\mu}_{Fe}(x) = \sum_{n=n_c}^{6} \sum_{m=0}^{12} \mu_{Fe}(n, m) P_1(n) P_2(m) \tag{3}$$

where $P_1(n)$ and $P_2(m)$ are binomial distribution functions for the first and second coordination shells, respectively. Performing the summation yields

$$\bar{\mu}_{Fe}(x) = (6\mu_1 + 12\mu_2)\, x - n_c\mu_1 + \mu_1 \sum_{n=0}^{n_c-1} (n_c - n) P_1(n). \tag{4}$$

The experimental $\bar{\mu}_{Fe}$ versus x data do not allow the three adjustable parameters in equation (4) to be uniquely determined, since the best fit to the data yields a different

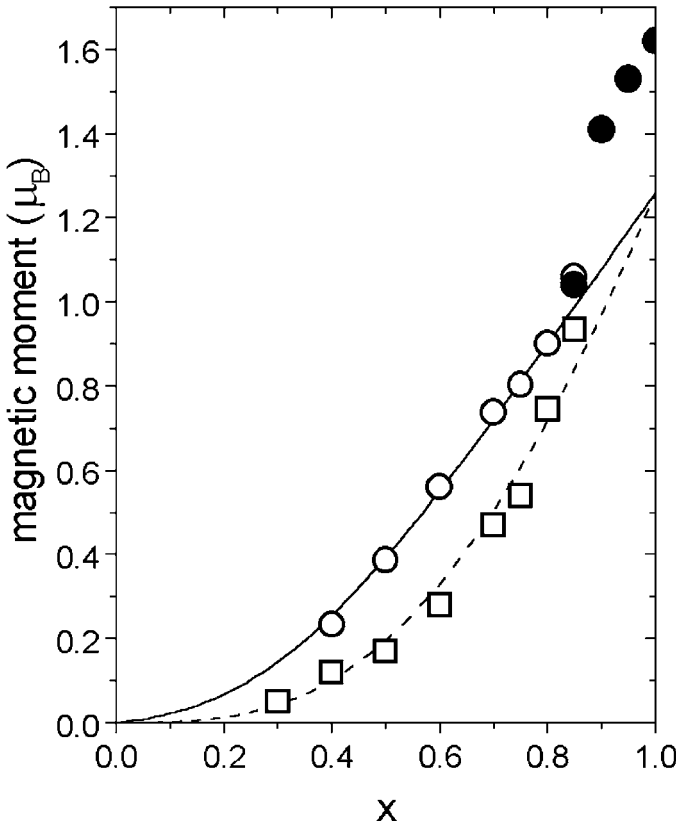

Figure 6. Fe magnetic moment versus x: experimental (open circles), calculated $\bar{\mu}_{\mathrm{Fe}}$ (full curve). Saturation moment/3d atom versus x: experimental μ_{s} (open squares: this work, filled circles: Reference [7]), calculated $x\bar{\mu}_{\mathrm{Fe}}$ (dashed curve).

(μ_1, μ_2) pair for every allowable choice of the integer n_{c}. By making the physically reasonable assumption that the μ_2/μ_1 ratio should be as small as possible (and positive), the best choice is $n_{\mathrm{c}} = 2$, when one obtains $\mu_1 = 0.27$ and $\mu_2 = 0.015$ Bohr magnetons per Fe neighbour. The calculated $\bar{\mu}_{\mathrm{Fe}}$ versus x curve has been included in figure 6. Agreement with experimental data is good, except at the lowest Fe concentrations. For the latter, however, the $T = 4.2$ K Mössbauer results underestimate the true Fe moment because the freezing temperature T_{f} becomes low (see section 3.3). Additionally, it can be seen in figure 6 that the concentration dependence of the average moment per 3d atom is given, within $\pm 0.05\ \mu_{\mathrm{B}}$, by $\mu_{\mathrm{s}} = x\bar{\mu}_{\mathrm{Fe}}$. Since $\mu_{\mathrm{s}} = (1-x)\bar{\mu}_{\mathrm{Cr}} + x\bar{\mu}_{\mathrm{Fe}}$ in general, this result is consistent with a null Cr moment. On the other hand, the model breaks down at $x = 0.85$ and higher concentrations, where the Fe moment rises much more steeply than predicted. It should be noted, however, that the data for $x > 0.85$ belong to the C15 phase stability range [7]. More detailed work would be necessary to determine whether the magnetic moment change upon crossing the C14–C15 boundary is discontinuous as in $Zr(Fe_{1-x}Al_x)_2$ [4], or smooth as the present data seem to indicate.

An independent test of the proposed local environment model is provided by the hyperfine field distributions deduced from the Mössbauer spectra. In view of the previous discussion, it is reasonable to assume the proportionality between B_{hf} and μ_{Fe} to hold for every particular

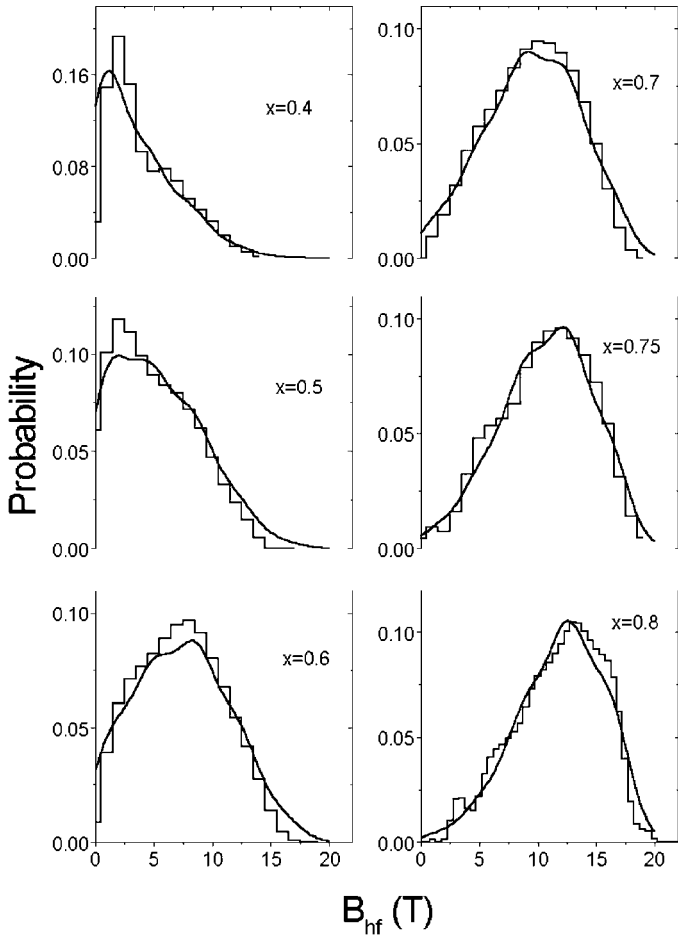

Figure 7. Calculated (smooth curves) and experimental (histograms) $P(B_{\rm hf})$ distributions.

environment, i.e. $B_{\rm hf}(n,m) = A\mu_{\rm Fe}(n,m)$ with $A = 13.2$ T$/\mu_{\rm B}$. In this way, the hyperfine field distribution can be calculated as

$$P(B) = \sum_{n,m} P_1(n)P_2(m)\exp\left\{-[B - B_{\rm hf}(n,m)]^2/2\sigma^2\right\}. \tag{5}$$

The discrete $B_{\rm hf}$ values have been convoluted with Gaussian profiles of width σ to account for the effect of more distant neighbour shells [21]. Experimental and calculated (with $\sigma = 1.7$ T) $P(B_{\rm hf})$ curves are compared in figure 7, showing excellent agreement. According to our model, the low-field $P(B_{\rm hf})$ peak seen for $x = 0.4$ and 0.5 can be assigned to Fe atoms with $0 \leqslant n \leqslant 2$, such that a small moment is induced only by second-neighbour Fe atoms. The fraction of Fe atoms with such environments is significant at these concentrations (54 and 34% for $x = 0.4$ and 0.5, respectively). Another distinctive feature of $P(B_{\rm hf})$ is the existence of a cut-off field $\sim$18 T: specifically, the observed increase in $\bar{B}_{\rm hf}$ with increasing x results from the shift of maximum $P(B_{\rm hf})$ towards larger fields, rather than from a uniform scaling to higher $B_{\rm hf}$ values. In contrast to this behaviour, the $B_{\rm hf}$ distributions for $Cr_{1-x}Fe_x$ alloys exhibit a cut-off field which increases steadily with Fe concentration [21]. The $Zr(Cr_{1-x}Fe_x)_2$ behaviour in this respect can be readily explained, according to our model, by the existence of a

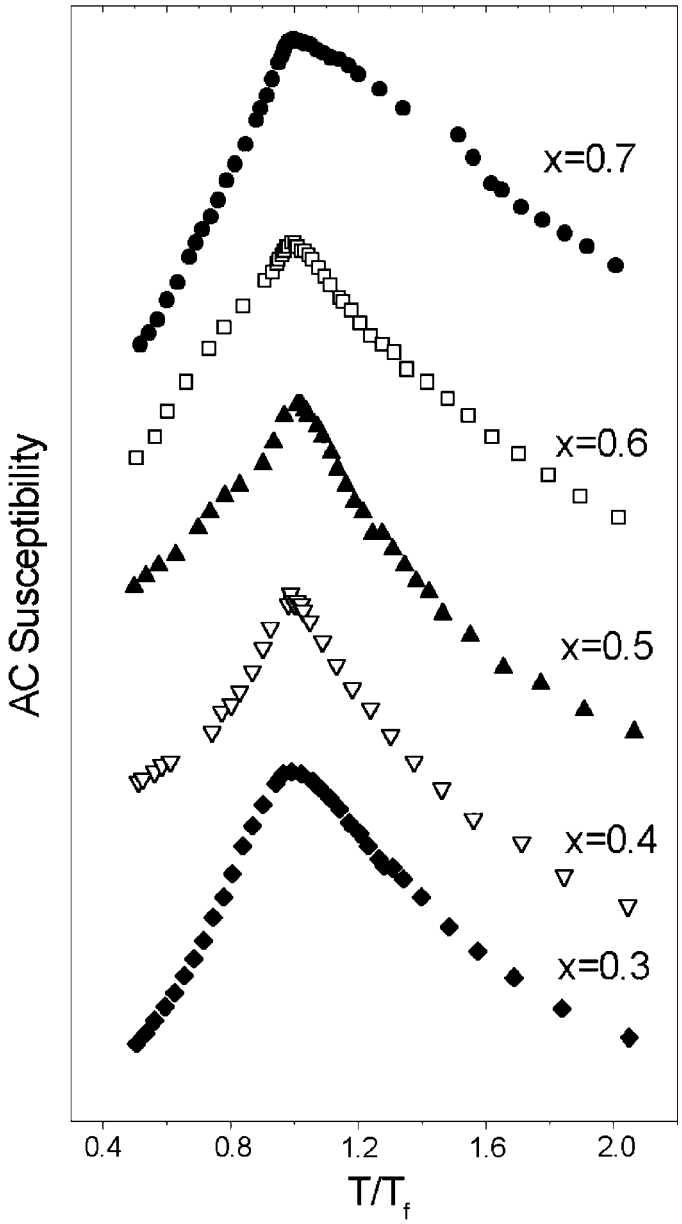

Figure 8. AC susceptibility versus reduced temperature. T_f values are given in table 1.

maximum Fe moment μ_{Fe} ($n = 6$, $m = 12$) $= 1.26\,\mu_B$, hence a maximum field $B_{hf}^{max} = 16.6$ T, independent of x.

3.3. Spin glass regime: $x \leqslant 0.7$

The alloys in this concentration range exhibit spin freezing with many characteristic features of a spin glass. The low-field ac susceptibility (measured at 155 Hz) shows a sharp peak at a temperature T_f, which increases with Fe concentration. As figure 8 shows, the shape of this

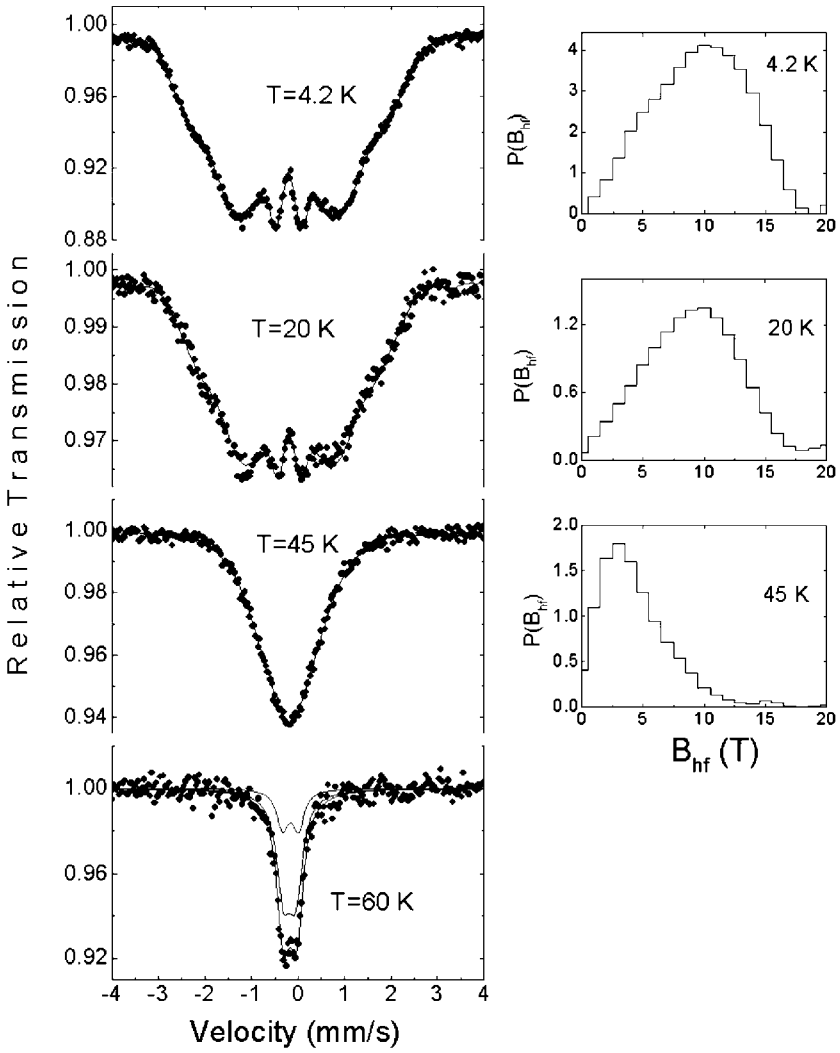

Figure 9. Mössbauer spectra of $Zr(Cr_{0.3}Fe_{0.7})_2$ and fitted $P(B_{\rm hf})$ at indicated temperatures.

peak as a function of reduced temperature $T/T_{\rm f}$ is similar for all concentrations. The freezing temperatures for $x = 0.3$ to 0.7 are given in table 2. It is of interest to note that $T_{\rm f}$ scales with the Fe moment following a power law $T_{\rm f} \sim (\bar{\mu}_{\rm Fe})^n$ with $n \approx 1.3$.

The appearance of magnetic hyperfine splitting in the Mössbauer spectra is another signature of spin freezing. A few spectra for $x = 0.7$, taken at representative temperatures, are shown in figure 9 together with the corresponding $P(B_{\rm hf})$ distributions. The spectrum at $T = 60$ K is non-magnetic and has been fitted with two overlapping quadrupole doublets, corresponding to the $2a$ and $6h$ Fe sites (see [17] for details). The average hyperfine field temperature dependence for samples with $x = 0.4$ to 0.7 is shown in figure 10. A 'Mössbauer freezing temperature' $T_{\rm f}^{\rm MS}$ is defined by the collapse of $\bar{B}_{\rm hf}$ (see table 2). As is often observed, $T_{\rm f}^{\rm MS}$ is higher than the $T_{\rm f}$ defined from the susceptibility peak. This shift, which results from the different time scales of the two kinds of experimental method, reflects time effects associated to the spin-glass freezing.

Table 2. Concentration dependence of quantities related to the spin glass phase: susceptibility peak temperature T_f, Mössbauer freezing temperature T_f^{MS}, Vogel–Fulcher parameters T_0 and E_a, critical slowing-down parameters T_g and $z\nu$.

x	0.3	0.4	0.5	0.6	0.7
T_f (K)	3.27(5)	10.5(1)	20.5(1)	32.1(1)	45.6(1)
T_f^{MS} (K)	—	13(2)	26(2)	39(2)	57(2)
T_0 (K)	1.3(2)	7.6(5)	15.6(1)	25(1)	37(1)
E_a/k (K)	49(4)	67(12)	123(3)	173(30)	210(14)
T_g (K)	2.5(1)	9.2(1)	18.5(2)	29.0(2)	43.0(2)
$z\nu$	10.1(7)	11.4(8)	10.6(1)	10.8(7)	8.6(5)

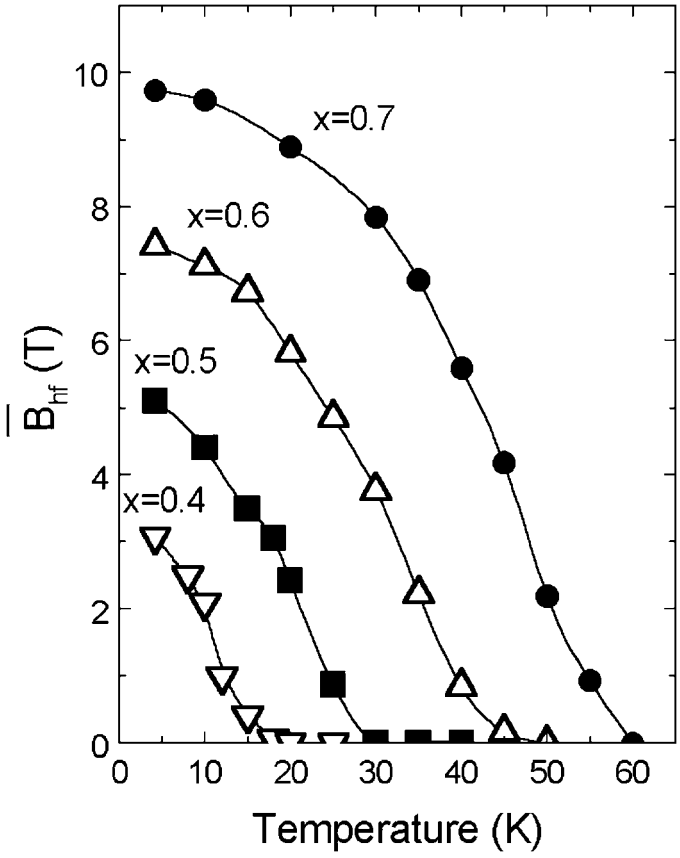

Figure 10. Temperature dependence of $Zr(Cr_{1-x}Fe_x)_2$ average hyperfine field, $x \leqslant 0.7$

The Vogel–Fulcher law

$$\tau(T) = \tau_0 \exp\left[\frac{E_a}{k(T - T_0)}\right] \tag{6}$$

is a popular device for describing time-dependent effects in spin glasses [22]. For a given measuring time τ_m, the freezing temperature is determined by the condition $\tau(T_f) = \tau_m$. AC susceptibility measurements have been carried out at various frequencies for all studied

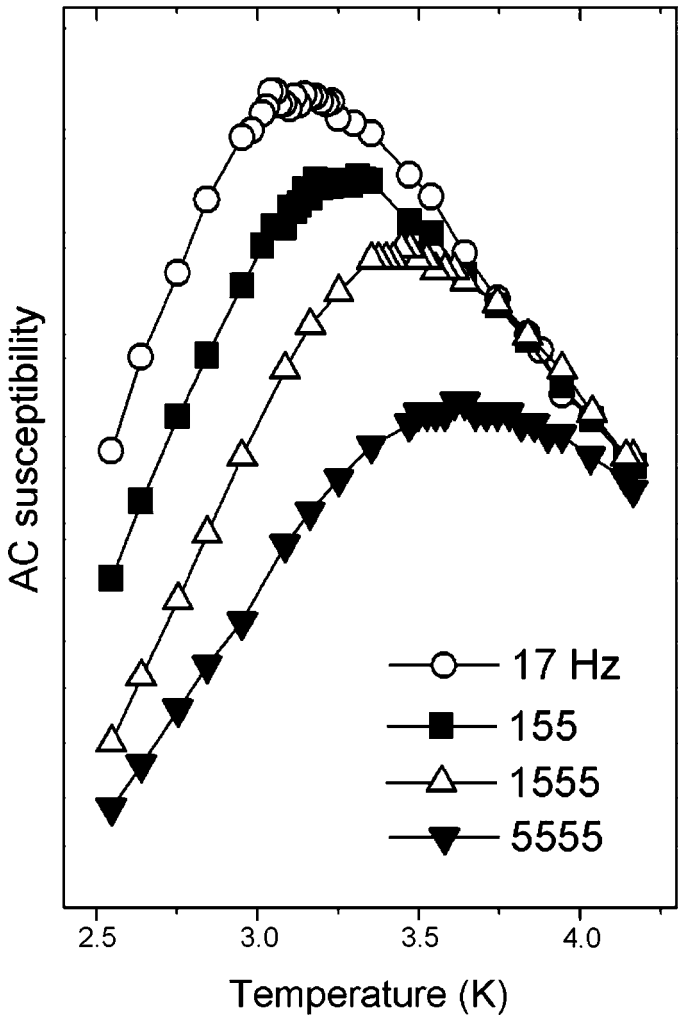

Figure 11. AC susceptibility of $Zr(Cr_{0.7}Fe_{0.3})_2$ at different measuring frequencies.

samples. The peak position shift with varying measuring time is illustrated in figure 11. Equation 6 has been used to fit the T_f versus frequency data, with τ_0 fixed at 10^{-13} s, and the resulting parameters E_a and T_0 are given in table 2 as a function of concentration. Both E_a and T_0 extrapolate to zero at $x \sim 0.25$. It is noteworthy that, by inserting the Mössbauer measuring time ($\tau_{MS} \sim 10^{-8}$ s) into equation (6) together with the fitted parameters E_a and T_0 for each concentration, Mössbauer freezing temperatures are calculated which agree very well with the measured ones.

An alternative description of the dynamics of the spin glass transition is given by the critical slowing-down power law [23]

$$\tau = \tau_0 \left(\frac{T_f - T_g}{T_g} \right)^{-z\nu} \tag{7}$$

Our T_f versus frequency data have been fitted with equation (7). Good fits could be obtained if τ_0 was left free to vary, yielding values in the $10^{-12.7\pm0.3}$ s range (except $\tau_0 = 10^{-7.3}$ s for

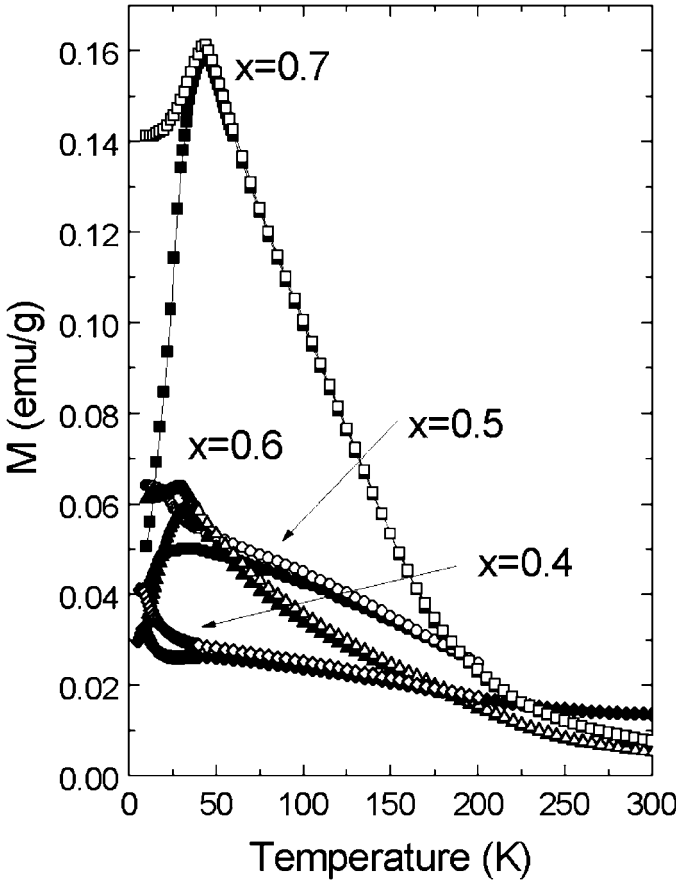

Figure 12. Zero field-cooled (open symbols) and field-cooled (filled symbols) magnetization data for $x \leqslant 0.7$ ($H_{app} = 100$ Oe).

$x = 0.3$). The resulting fit parameters T_g and $z\nu$ are given in table 2. The critical index $z\nu$ is consistent with literature values [24–26], usually found to be around 8–10, though somewhat smaller values (∼7) are expected from numerical simulations [27].

At this point the question arises whether the materials under study are 'good spin glasses', i.e. whether a cooperative freezing transition occurs at a definite temperature, as opposed to superparamagnetic cluster relaxation. A thumb rule proposed by Tholence [28] uses the quantity $(T_f - T_0)/T_f$ [or, equivalently, $E_a/kT_f \ln(\tau_m/\tau_0)$] as an index that runs from low values (∼0.04) for canonical spin glasses, to ∼1 for superparamagnets. Applying this criterion to the Vogel–Fulcher parameters in table 2, one sees that the most concentrated alloy $x = 0.7$ comes closest to the ideal spin glass case. Alternatively, the relative T_f increment per frequency decade is an empirical figure of merit for spin glasses. Again, the lowest $(\Delta T_f/T_f)/\Delta \log_{10} \omega$ value (=0.021) is found for the $x = 0.7$ alloy.

The above conclusion is corroborated by the ZFC/FC magnetization data shown in figure 12. Two characteristic temperatures can be defined: T_f at the peak, and T_{irr} where the two curves part. For $x = 0.7$, T_f and T_{irr} nearly coincide, resembling the behaviour of AuFe, CuMn etc. For decreasing x, however, the gap between T_f and T_{irr} increases, revealing the growing importance of the individual blocking of clusters of different sizes.

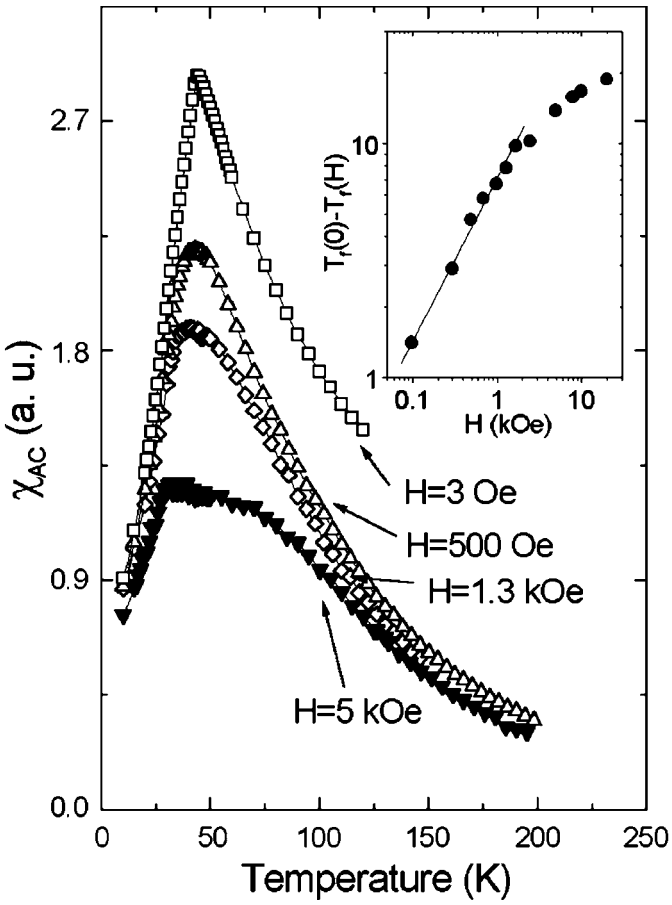

Figure 13. AC susceptibility of $Zr(Cr_{0.3}Fe_{0.7})_2$ at different applied DC fields. Inset: peak shift versus field; fitted exponent $c = 0.68$.

Figure 13 shows the field dependence of the ac susceptibility of $Zr(Cr_{0.3}Fe_{0.7})_2$. Although the T_f peak is depressed by the applied field in the usual way, a maximum can be identified for fields as large as 20 kOe. It is noteworthy that the peak is shifted towards lower temperatures upon applying a field. An attempt to describe this behaviour with a power law $T_f(0) - T_f(H) = aH^c$ has yielded the exponent $c = 0.68(3)$ for fields not exceeding 1 kOe (see inset).

3.4. Ferromagnetic/re-entrant spin glass: $x > 0.7$

As was noted in section 3.2, the Arrott plots at 4.2 K indicated ferromagnetic ordering for $Zr(Cr_{1-x}Fe_x)_2$ alloys with $x > 0.7$. The evolution from spin glass to long-range ferromagnetism in concentrated alloys is commonly viewed as a special kind of percolation process, which results in the development of an infinite cluster of nearest-neighbour ferromagnetic bonds. Once the percolation concentration has been reached, the ordering temperature rises steeply with increasing concentration of the magnetic element.

Figure 14 shows the temperature dependence of the mean hyperfine field for samples with $x \geqslant 0.7$. From the above considerations it is clear that the hyperfine field collapse signals the

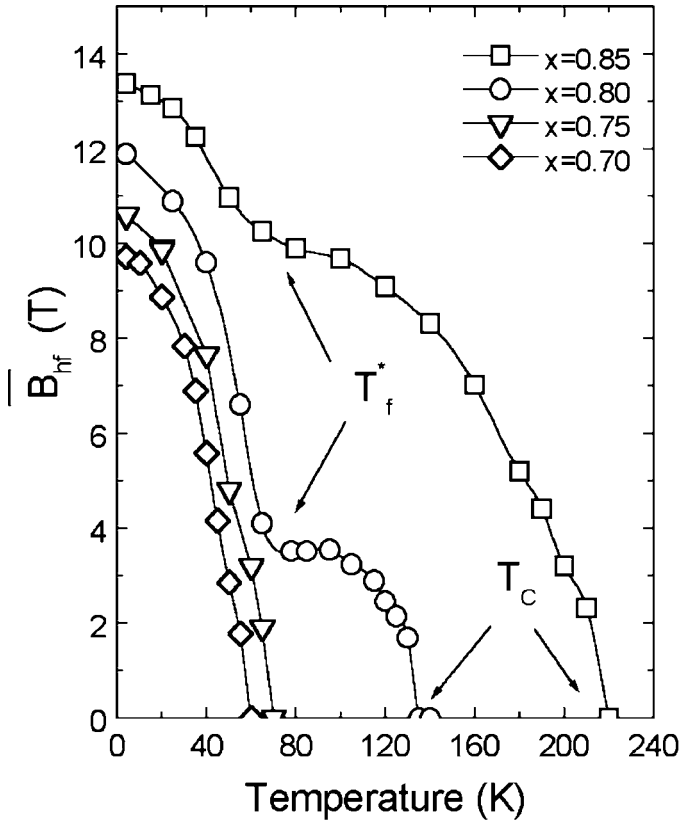

Figure 14. Temperature dependence of $Zr(Cr_{1-x}Fe_x)_2$ average hyperfine field, $x \geqslant 0.7$.

Curie temperature of the $x = 0.75$–0.85 alloys. The T_C value thus obtained for $Zr(Cr_{0.15}Fe_{0.85})_2$ (220 K) agrees well with published magnetization data [7].

For the $x = 0.8$ and 0.85 alloys a second transition is evident at a lower temperature T_f^*, revealed by a kink in the $\bar{B}_{hf}$ versus T curves. This double-transition behaviour, which defines a re-entrant spin glass (RSG), characterises the crossover to ferromagnetism in many spin glass systems just above the percolation threshold. Its characteristic features are usually seen in low-field susceptibility data. Figure 15 shows ZFC and FC magnetisation versus temperature data taken in $H_{app} = 100$ Oe. The $x = 0.85$ curve exhibits a typical plateau-like shape, somewhat less evident for $x = 0.80$. The T_C's determined from Mössbauer spectra coincide with the fast magnetization rise for descending temperatures, while the second transition temperature T_f^* is close to the ZFC curve maximum.

The physical basis for the RSG behaviour is still controversial. One model [29] attributes the T_f^* transition to the freezing of small magnetic clusters coexisting with the infinite cluster. Another one, based on a mean-field Heisenberg model [30], assumes the spin components normal to the ferromagnetic $\langle S_z \rangle$ to freeze at T_f^*. It appears that the transverse spin freezing, rather than the cluster model, has been substantiated in all cases where a spin direction-sensitive probe like Mössbauer spectroscopy could be applied to this problem (e.g. AuFe [31], $(Fe_{65}Ni_{35})_{1-x}Mn_x$ [32], a-Fe_xZr_{1-x} [33]).

The ZFC/FC curves for the $x = 0.8$ sample are somewhat unusual in that irreversibility starts at a temperature, $T_{irr} \sim 50$ K, which is well below T_f^*. Magnetization loops have been

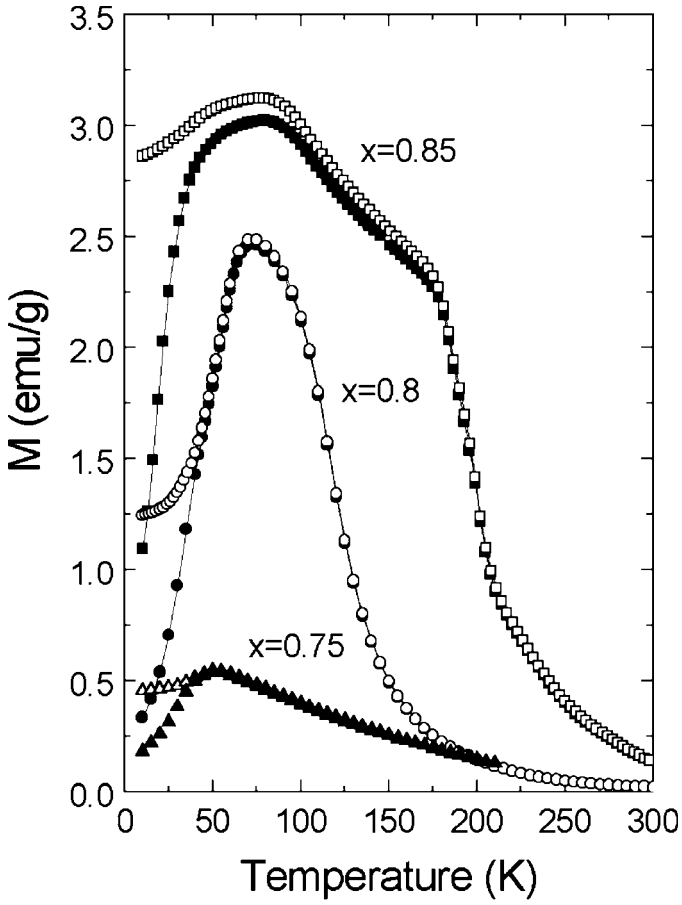

Figure 15. Zero field-cooled (open symbols) and field-cooled (filled symbols) magnetization data for $x \geqslant 0.75$ ($H_{app} = 100$ Oe).

traced to explore this behaviour further, a few being displayed in figure 16. The inset shows the coercive field H_c as a function of temperature. The constant H_c value seen above 50 K may be to some extent an instrumental artefact, as it was found to persist above T_C. However, the strong increase from 25 K downwards is a genuine effect, which signals the onset of strong irreversible behaviour. A completely similar effect has been found earlier in an Au–19at.%Fe alloy, a re-entrant ferromagnet which shows a kink in the B_{hf} versus T curve similar to those in figure 14 [34]. The nature of this effect is not clear, but it has been suggested [34] that it constitute a manifestation of the Almeida–Thouless [35] crossover to strong irreversibility.

4. Conclusions

The main results of this work are summarized in the magnetic phase diagram of figure 17. At the iron-rich side, this diagram touches the boundary of the hexagonal C14 phase. Insofar as magnetic data for the adjoining C15-phase region are available [7], it seems that the ferromagnetic Curie temperature undergoes a discontinuous jump upon changing the crystal

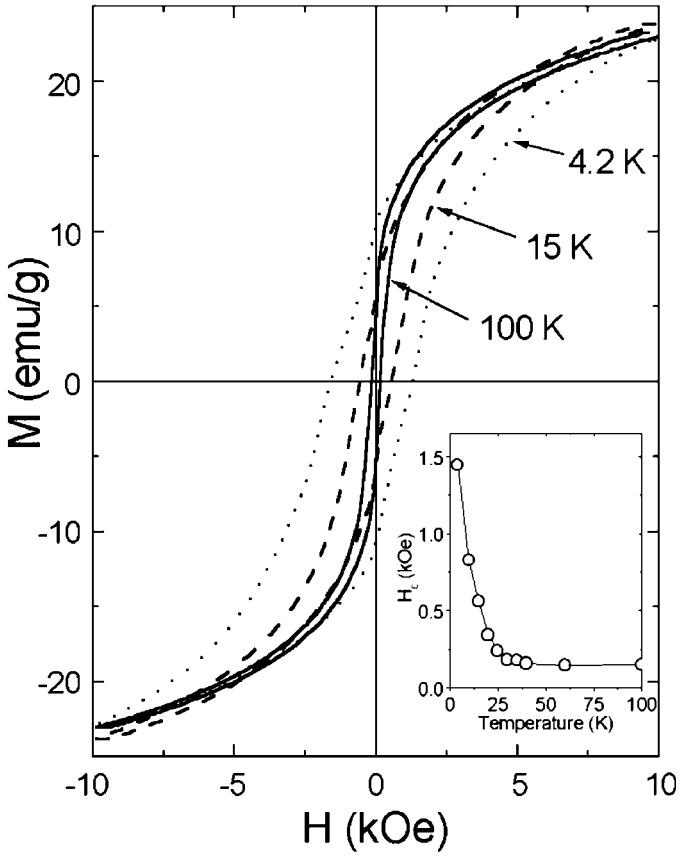

Figure 16. Hysteresis loops of $Zr(Cr_{0.2}Fe_{0.8})_2$ at various temperatures. Inset: coercive field versus temperature.

structure. It is not known whether the reentrant spin glass phase extends into the C15-phase region.

It is interesting to compare the results of this work with other pseudobinary Zr(Fe, M)$_2$ compounds. Among the well-documented systems with $M =$ Mn, Co, Ni, Al [4, 6, 36], $M =$ Al is most appropriate for comparison with the Cr alloys because $Zr(Fe_{1-x}Al_x)_2$ also crystallizes in the C14 structure for a wide concentration range ($x > 0.25$). The latter compounds exhibit long-range magnetic order up to $x_c = 0.55$, at which concentration both T_C and the Fe moment vanish; accordingly, no spin-glass-like freezing was ever observed in this system [4]. In contrast, $Zr(Fe_{1-x}Cr_x)_2$ features a faster disappearance of long-range magnetic order with increasing x ($T_C \rightarrow 0$ at $x = 0.3$) and, at the same time, much more persistent magnetic moments (indeed, two Fe neighbours are sufficient to stabilize a small Fe moment); as a consequence, the magnetic phase diagram shows an exceptionally broad spin-glass-phase concentration range. In this respect, $Zr(Fe,Cr)_2$ is qualitatively similar to $Y(Fe,Al)_2$, which has been characterized as a localized moment system, in contrast with the itinerant magnetism of $Zr(Fe,Al)_2$ [4, 36]. On the other hand, from the point of view of the effect of chemical substitution on the magnetism of $ZrFe_2$, it can be said that Cr is more effective than Al in destroying magnetic order, but the reverse is true with respect to the Fe magnetic moments.

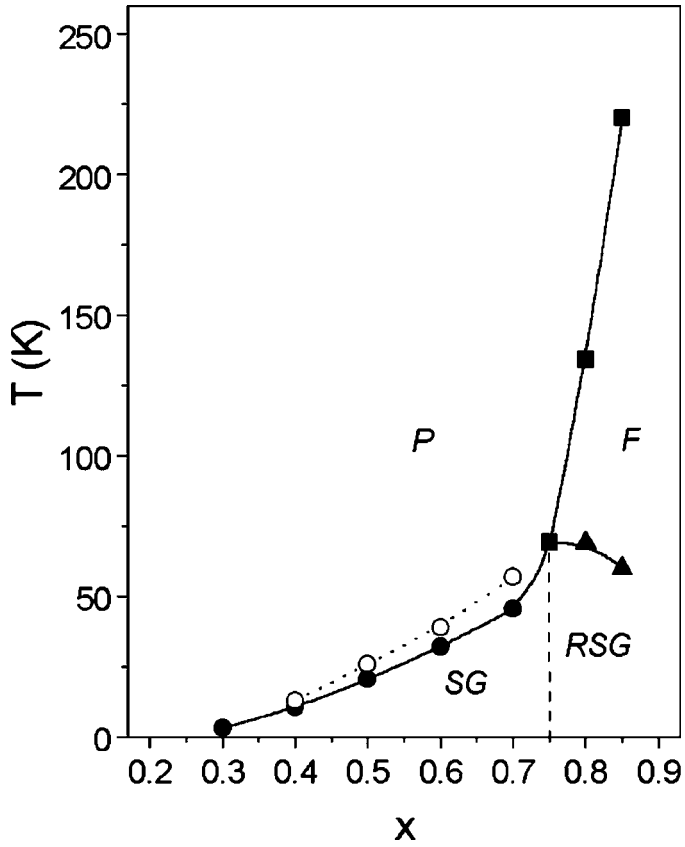

Figure 17. Magnetic phase diagram of C14-type $Zr(Cr_{1-x}Fe_x)_2$. Filled circles: T_f, open circles: T_f^{MS}, squares: T_C, triangles: $T_f{}^*$.

Another line of discussion concerns the magnetic behaviour of Fe–Cr random mixtures in different structures. Boliang *et al* [37] have discussed the differences between crystalline $Fe_{1-x}Cr_x$ alloys [13] and Fe–Cr-based metallic glasses typified by $(Fe_{1-x}Cr_x)_{80}B_{20}$ [14]. In the former, T_C decreases slowly with increasing x and Fe atoms retain a well-defined moment over a large concentration range. In the amorphous alloys, T_C falls much more rapidly with increasing x and the Fe moment follows the same trend; thus, the onset of magnetic order coincides with the appearance of a moment on Fe atoms, in a way resembling $Zr(Fe,Al)_2$. From the preceding discussion, it is clear that the magnetic behaviour of $Zr(Fe,Cr)_2$ lies between these extreme cases of localized and itinerant magnetism.

Acknowledgments

This work was financially supported by FAPESP. Research fellowships from FAPESP (J A H C) and CNPq (H R R) are gratefully acknowledged.

References

[1] Taylor K N R 1971 *Adv. Phys.* **20** 551
[2] Buschow K H J 1977 *Rep. Prog. Phys.* **40** 1179

[3] Steiner W 1979 *J. Magn. Magn. Mater.* **14** 47
[4] Hilscher G 1982 *J. Magn. Magn. Mater.* **27** 1
[5] Yamada H 1988 *Physica* B **149** 390
[6] Muraoka Y, Shiga M and Nakamura Y 1979 *J. Phys. F: Metal Phys.* **9** 1889
[7] Kanematsu K and Fujita Y 1970 *J. Phys. Soc. Japan* **29** 864
[8] Shaltiel D, Jacob I and Davidov D 1977 *J. Less-Common Met.* **53** 117
[9] Jacob I, Davidov D and Shaltiel D 1980 *J. Magn. Magn. Mater* **20** 226
[10] Fujii H, Pourarian F and Wallace W E 1982 *J. Less-Common Met.* **88** 187
[11] Wallace W E, Pourarian F, Pedziwiatr A T and Boltich E B 1987 *J. Less-Common Met.* **130** 33
[12] Kanematsu K 1971 *J. Phys. Soc. Japan* **31** 1355
[13] Burke S K and Rainford B D 1983 *J. Phys. F: Metal Phys.* **13** 441 and 471
Burke S K, Cywinski R, Davis J R and Rainford B D 1983 *J. Phys. F: Metal Phys.* **13** 451
[14] Olivier M, Ström-Olsen J O, Altounian Z and Williams G 1982 *J. Appl. Phys.* **53** 7696
[15] Yeshurun Y, Rao K V, Salamon M B and Chen H S 1981 *Solid State Commun.* **38** 371
[16] Canet O, Latroche M, Bourée-Vigneron F and Percheron-Guégan A 1994 *J. Alloys Compds.* **210** 129
[17] Coaquira J A H, Rechenberg H R and Mestnik Filho J 1999 *J. Alloys Compds.* **288** 42
[18] Besnus M J, Bauer P and Génin J M 1978 *J. Phys. F: Metal Phys.* **8** 191
[19] Amaral L, Livi F P and Gomes A A 1982 *J. Phys. F: Metal Phys.* **12** 2091
[20] Jaccarino V and Walker L R 1965 *Phys. Rev. Lett.* **15** 258
[21] Shiga M and Nakamura Y 1980 *J. Phys. Soc. Japan* **49** 528
[22] Tholence J L 1980 *Solid State Commun.* **35** 113
[23] Hohenberg P C and Halperin B I 1977 *Rev. Mod. Phys.* **49** 435
[24] Svedlindh P, Lundgren L, Nordblad P and Chen H S 1987 *Europhys. Lett.* **3** 243
[25] Gunnarsson K, Svedlindh P, Nordblad P, Lundgren L, Aruga H and Ito A 1988 *Phys. Rev. Lett.* **61** 754
[26] Djurberg C, Svedlindh P, Nordblad P, Hansen M F, Bødker F and Mørup S 1997 *Phys. Rev. Lett.* **79** 5154
[27] Ogielski A T 1985 *Phys. Rev.* B **32** 7384
[28] Tholence J L 1984 *Physica* B **126** 157
[29] Coles B R, Sarkissian B V B and Taylor R H 1978 *Phil. Mag.* B **37** 489
[30] Gabay M and Toulouse G 1981 *Phys. Rev. Lett.* **47** 201
[31] Lauer J and Keune W 1982 *Phys. Rev. Lett.* **48** 1850
[32] Huck B and Hesse J 1989 *J. Magn. Magn. Mater.* **78** 247
[33] Ryan D H 1992 *Recent Progress in Random Magnets* ed D H Ryan (Singapore: World Scientific) p 1
[34] Campbell I A, Senoussi S, Varret F, Teillet J and Hamzic A 1983 *Phys. Rev. Lett.* **50** 1615
[35] de Almeida J R L and Thouless D J 1978 *J. Phys.* A **11** 983
[36] Muraoka Y, Shiga M and Nakamura Y 1977 *Phys. Status Solidi* A **42** 369
[37] Boliang Y, Coey J M D, Olivier M and Ström-Olsen J O 1984 *J. Appl. Phys.* **55** 1748